Anhydride-containing oligomer-crosslinked gelatin microparticles: crosslinking process understanding using design of experiments

Burak Demir, Johannes Reiss, Julia C. Matros, Stefan Klinken-Uth, Michael C. Hacker

Results in Engineering 29 (2026) 109860

Contents lists available at ScienceDirect

Results in Engineering

journal homepage: www.sciencedirect.com/journal/results-in-engineering

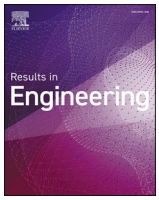

Research paper

Anhydride-containing oligomer-crosslinked gelatin microparticles: crosslinking process understanding using design of experiments

Burak Demir [a], Johannes Reiss [a,b], Julia C. Matros [a], Stefan Klinken-Uth [a], Michael C. Hacker [a,*]

[a] Faculty of Mathematics and Natural Sciences, Institute of Pharmaceutics and Biopharmaceutics Universitaetsstrasse 1, Heinrich Heine University Duesseldorf, Duesseldorf 40225, Germany
[b] INVITE GmbH, Formulation Technology, Otto-Bayer-Strasse 32, Koeln 51061, Germany

ARTICLE INFO

Keywords:
Anhydride copolymers
Maleic anhydride
Protein microspheres
Design of experiments
Gelatin crosslinking
Process understanding

ABSTRACT

Crosslinked gelatin microparticles (cGM) are versatile biomaterials with applications in regenerative medicine, tissue engineering, and drug or gene delivery. In this study, we investigated the crosslinking process of pristine gelatin microparticles using new generation reactive anhydride-containing amphiphilic oligomers synthesized from stearyl acrylate, 4-acryloylmorpholine, and maleic anhydride at varying ratios. An optimal design of experiments (DoE) was employed, comprising three factors and three responses. The factors included the anhydride content applied per crosslinking reaction (AC), the volume of base, i.e. triethylamine (TEA), and the molecular anhydride distribution (MAD) of a given oligomer type, an indirect parameter reflecting the stoichiometric density of anhydride units along the oligomer chains. The responses consisted of the mean degree of crosslinking (DoC) of the particle batch, degree of swelling (DoS), and particle transparency (MT). Dynamic image analysis and light micrographs confirmed the spherical morphology of the crosslinked gelatin microparticles and demonstrated that the crosslinking step did not alter particle shape. Through DoE runs, cGM batches with a broad range of crosslinking densities (DoC: 34–79%) were achieved. AC exerted the strongest effect on DoC and DoC correlated with AC following a logarithmic regression. An overall correlation between DoC and DoS was evident, showing that higher crosslinking densities reduced particle swelling. The TEA volume applied during crosslinking indicated that only small amounts were still sufficient to obtain a wide range of DoC, which is a favorable outcome as minimizing TEA helps reduce potential adverse effects in the final material. Finally, through DoE study, we established that oligomer MAD as a critical material attribute for this process, as it significantly influenced all responses.

1. Introduction

Over the years, gelatin-based microparticles have emerged as versatile biomaterials, demonstrating utility in a wide range of pharmaceutical applications, including the delivery of conventional drugs [1–4], cells [5–7], proteins [8–12], and nucleic acids [13–17]. In addition, gelatin-based microparticles have gained increasing relevance in regenerative medicine and tissue engineering, serving as particulate templates for tissue assemblies [7,12–14,18–20]. However, the poor thermal and hydrolytic stability of gelatin represents a major limitation for its applications, necessitating crosslinking of the gelatin-based particles [21].

To date, different types of crosslinkers have been utilized to crosslink gelatin [3,9,10,22–26]. Crosslinking can be achieved in two different ways: physically or chemically [21]. Gelatin can be physically crosslinked via electron beam irradiation, plasma treatment or dehydrothermal treatment [22,27]. However, physical crosslinking is usually not an efficient process and offers limited control of crosslinking density. In contrast, chemical crosslinking involves the formation of covalent bonds, offering advantages in controlling crosslinking density and tailoring the final material properties of gelatin. Chemical crosslinkers can be classified as i) zero-length crosslinkers, which do not become part of the final material, and ii) non-zero-length crosslinkers, which covalently crosslink gelatin chains and remain integrated into the final structure [21]. Zero-length crosslinkers, such as carbodiimide derivatives, offer advantages because the leaching of non-zero-length

* Corresponding author.
E-mail address: michael.hacker@hhu.de (M.C. Hacker).

https://doi.org/10.1016/j.rineng.2026.109860
Received 27 February 2026; Accepted 1 March 2026
Available online 2 March 2026

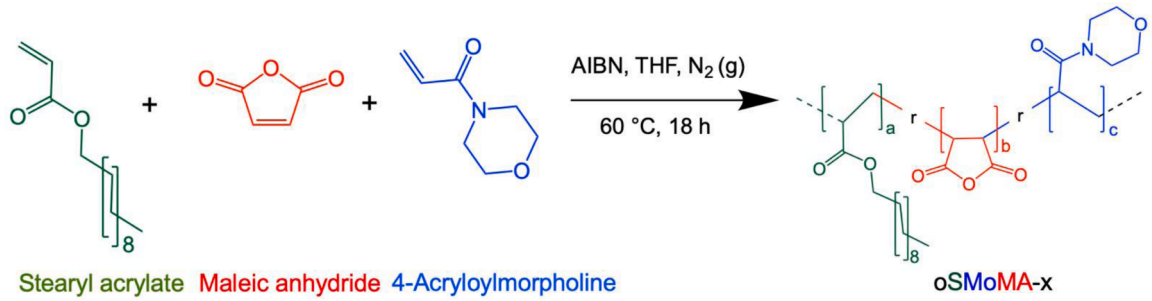

Fig. 1. Chemical illustration of the synthesis of anhydride-containing random copolymeric oligomers. The reaction medium consists of comonomers and AIBN, as a radical initiator. Anhydrous THF was used as a reaction solvent. The reaction was proceeded at 60 °C for 18 h under continuous N_2 (g) purge.

crosslinkers like glutaraldehyde (GTA) during biodegradation may cause toxic effects. However, they often result in fast biodegradation rates [28]. Genipin, a naturally occurring crosslinker, is considered a good alternative to GTA due to its lower toxicity and comparable crosslinking efficiency. Nevertheless, its relatively high cost and typically long reaction times remain challenges for its application [29]. On the other hand, anhydride-containing oligomeric crosslinkers offer several advantages, including their good biocompatibility, ability to achieve high crosslinking densities, and flexibility for chemical modification via anhydride functionalities to tailor final material properties [30]. Moreover, their synthesis provides substantial flexibility in controlling and tuning key chemical characteristics of the crosslinker, such as molecular weight, copolymer composition and reactive anhydride content [24,31,32]. While some of these crosslinkers have previously been employed to crosslink pristine gelatin microparticles (GM) [13,14,23], systematic statistical investigations following controlled experimental designs that provide crosslinking process understanding and identify key material attributes of the crosslinkers are still lacking.

In this study, we investigated the crosslinking process of pristine GM, fabricated via a water-in-oil (W/O) emulsion technique [33], using our new-generation anhydride-containing oligomeric crosslinkers composed of stearyl acrylate (SA), 4-acryloylmorpholine (AMO), and maleic anhydride (MA) at varying ratios. We employed an optimal DoE with three factors to assess their criticality in the crosslinking process and to enhance process understanding for anhydride-containing crosslinkers. The investigated factors included the total molar anhydride content (AC) introduced by a specific crosslinker, the base volume used in the reaction (TEA), and the molecular anhydride distribution (MAD) – an oligomer-specific parameter reflecting the stoichiometric density of anhydride units along the copolymeric chains. The mean degree of crosslinking (DoC) was used as the primary response variable to quantify the extent of covalent crosslinking of the gelatin matrix, while the degree of swelling (DoS) and particle transparency (MT) were evaluated as supportive responses, serving as indicators of network structure to support mechanistic interpretation of the crosslinking process.

2. Materials and methods

2.1. Materials

Stearyl acrylate (SA) (97 %, 200 ppm monomethyl ether hydroquinone), 4-acryloylmorpholine (AMO) (97 %, 1000 ppm MEHQ), anhydrous tetrahydrofuran (THF) (≥99.9 %, 250 ppm BHT), azobisisobutyronitrile (AIBN) (98 %), gelatin type B (~225 g Bloom), triethylamine (TEA) (≥99.5 %), sodium bicarbonate (≥ 99.7 %) and aqueous trinitrobenzenesulfonic acid (TNBS) solution (5 % (w/v)) were purchased from Merck KGaA (Darmstadt, Germany). Medium-chain triglycerides (MYRITOL® 318 now: Kollisolv® MCT 70) was purchased from Caesar & Loretz GmbH (Hilden, Germany) whereas maleic anhydride (MA) (99 %) was obtained from Fisher Scientific GmbH (Schwerte, Germany). Acetone and isopropanol were used in technical grade. 6 M hydrochloric acid (HCl) solution was purchased from Honeywell GmbH (Neuss, Germany) whereas phosphate buffered saline (PBS) powder was obtained from AppliChem GmbH (Darmstadt, Germany). Demineralized water was produced using a Barnstead™ MicroPure™ water purification system (Thermo Fisher Scientific GmbH, Dreieich, Germany).

2.2. Synthesis and characterization of oligomeric crosslinkers

Oligomeric crosslinkers were synthesized by free radical polymerization following a protocol similar to those previously described [24,31,32]. Briefly, to initiate the synthesis, the comonomers, including SA, AMO, and MA were dissolved in freshly distilled anhydrous THF. AIBN was then added as the radical initiator, and the reaction was carried out at 60 °C for 18 h under a continuous N_2 (g) purge (Fig. 1). At the end of the reaction, THF was removed by rotary evaporation to obtain a concentrated solution containing the final product. Purification was performed through three repeated cycles of diethyl ether precipitation, followed by vacuum drying as described before [24,31,32]. The purified oligomers were stored in a vacuum chamber until further use. Oligomer characterization was conducted using gel permeation chromatography (GPC), conductometric titration, and ^{1}H—NMR, as described previously [24,31,32].

The oligomers were designated as oSMoMA-x, with the naming based on the molar stoichiometric ratios of the comonomer feed used during synthesis. Specifically, the molar feed ratio of MA to SA was 5:1 in oSMoMA-5 and 7.5:1 in oSMoMA-7.5 etc. For all oligomer types, the molar feed ratio of SA to all remaining comonomers was maintained at 1:20, while the ratio of AIBN to the total comonomers was kept at 2 % [mol/mol]. oSMoMA-5, oSMoMA-7.5 and oSMoMA-10 were synthesized by introducing all comonomers into the reaction medium simultaneously. In contrast, for oSMoMA-10c, the reaction was first initiated with SA and MA, while AMO was gradually added over 2 h. This approach was intended to extend the initial polymer chains with additional anhydride units, ultimately yielding oligomers with a higher molecular anhydride content.

2.3. Fabrication of crosslinked gelatin microparticles

Crosslinked gelatin microparticles (cGM) were fabricated in a two-step process. First, pristine GM were produced by a W/O emulsion method using a fabrication set-up that consisted of a 400 ml borosilicate glass beaker (VWR Borosilicate Glass 3.3, 213–1125, VWR International GmbH, Germany), an overhead stirring drive (Eurostar 60 control, IKA-Werke GmbH & Co. KG, Staufen, Germany) equipped with a three-bladed propeller-type tool, and a heating plate (Hei-Tec, Heidolph Scientific Products GmbH, Schwabach, Germany). In the second step, GM were crosslinked with anhydride-containing oligomeric crosslinkers.

To fabricate pristine GM, a gelatin solution was prepared by dissolving 2.5 g of gelatin in 25 ml of demineralized water. This solution was then introduced into 200 ml of MCT. The mixture was emulsified at

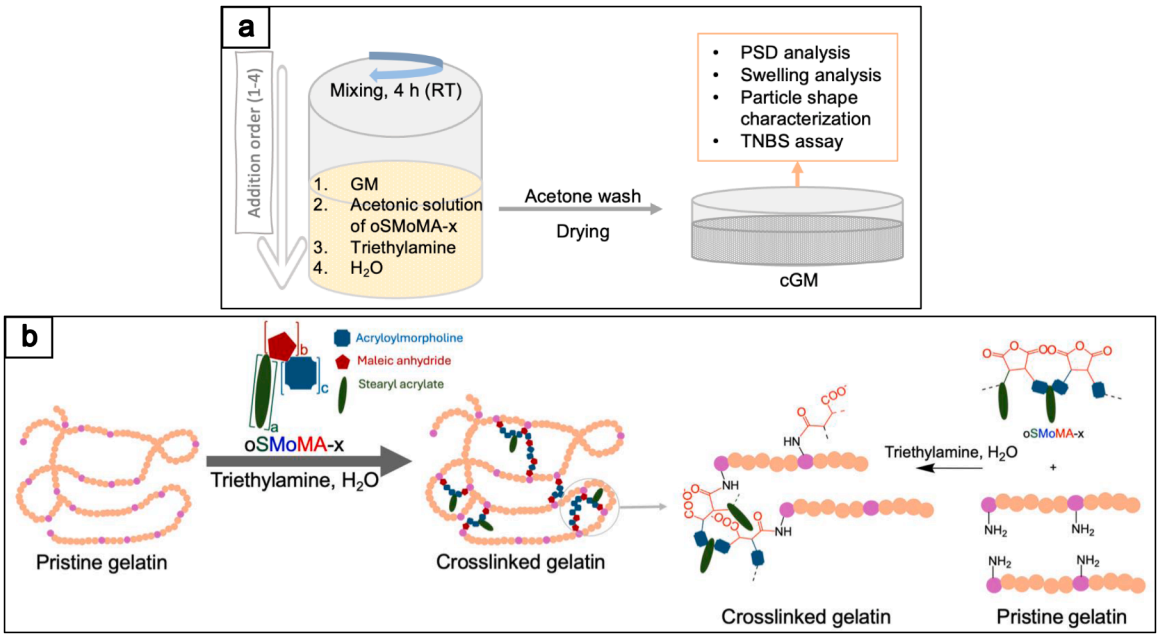

Fig. 2. (a) Illustration of cGM fabrication and characterization process. Reaction mixture contains pristine gelatin microparticles (GM), oSMoMA-x solution (dissolved in acetone), triethylamine (TEA) and demineralized water. Water was used to swell particles to facilitate oligomer penetration and assure crosslinking throughout the particle volume. Crosslinked particles were analyzed regarding particle size distribution (PSD), particle shape factors, swelling behavior and degree of crosslinking. (b) Chemical illustration of gelatin crosslinking through anhydride-amine conjugation reaction. Anhydride groups in oSMoMA-x react with primary amines in gelatin chains while TEA assures deprotonation of free amines to facilitate the nucleophilic attack.

50 °C and 700 rpm for 10 min. Subsequently, the heating plate was replaced with an ice bath, and sol-gel transformation was ensured by maintaining stirring for 30 min. To harden the particles, 100 ml of chilled acetone (technical-grade) was added while stirring continued for an additional 60 min [23,33]. The particles were then recovered, washed 5 times with acetone, and dried in a fume hood for 2 days, followed by an additional day of vacuum drying. Finally, the GM were sieved using a sieve with a 140 μm mesh size to remove large agglomerates. For the experimental design, a homogenous batch of GM was obtained by combining multiple GM batches fabricated under the same conditions.

In the second step, GM were crosslinked using anhydride-containing oligomers in an acetone water mixture providing sufficient solubility for the reactive crosslinker and a certain degree of solubilization of the particles without dissolving the particles assuring chemical access to gelatin's amine groups. Our crosslinking reaction is based on anhydride-amine conjugation chemistry, as previously described in the literature [13,14,23], where primary amine groups in gelatin chains were crosslinked with reactive anhydride units of the oligomeric crosslinkers. Prior to use in crosslinking, oligomer batches were incubated in an oven at 130 °C for 24 h to enhance anhydride reactivity, as recommended in literature [34]. GM crosslinking was conducted at two different scales: a large scale for preliminary batches and a downscaled version for the DoE batches, which was chosen for practical reasons. In the preliminary batches, 1 g of GM was initially wetted with 2 ml of acetone. Either 1 g or 2 g of oligomeric crosslinkers were dissolved in 18 ml of acetone and subsequently added to the GM. The final oligomer concentration relative to final acetone volume was 5 % [1 g oligomer in 20 ml acetone] and 10 % [2 g oligomer in 20 ml acetone], respectively. Immediately thereafter, 1 ml of TEA and 10 ml of demineralized water added to the mixture, respectively. Water was used to induce GM swelling, facilitating the diffusion of oligomers throughout the particle volume.

In DoE experimental series, 0.5 g of GM was initially wetted with 1 ml of acetone. The oligomeric crosslinker weight corresponding to the target AC was dissolved in 9 ml of acetone and added to the GM. Subsequently, the required volume of TEA and 5 ml of water were introduced sequentially into the reaction mixture. Independent of the setup, the reaction proceeded for 4 h at room temperature (RT), after which the cGM were recovered and washed multiple times with fresh acetone to remove unreacted oligomers and TEA. The final cGM were dried in a fume hood for one day, followed by an additional day of vacuum drying under conditions that are not considered to yield dehydrothermal crosslinking (Fig. 2a).

2.4. Particle characterization

2.4.1. Particle size and shape characterization

The particle size distribution (PSD) of fabricated cGM batches was characterized using laser diffraction (Mastersizer 3000 equipped with a Hydro SV dispersion unit, Malvern Panalytical GmbH, Kassel, Germany). Measurements were conducted for two particle states: non-swollen particles and PBS-swollen particles. For this, particles were dispersed in isopropanol for the non-swollen state and in phosphate-buffered saline (PBS) for the swollen state before diffraction analysis. Each batch was measured in triplicate by maintaining laser obscuration between 5–7 %, and results were expressed as a volume distribution using the Fraunhofer approximation. The de Brouckere mean diameter (D[4,3]) was used to determine the mean particle diameter for each cGM batch in both states. The degree of swelling (DoS) for each cGM batch was then calculated using Eq. (1) as previously reported in the literature [23].

$$DoS = \left(\frac{D[4,3]_{PBS} - D[4,3]_{isopropanol}}{D[4,3]_{isopropanol}} \right) \quad (1)$$

Particle shape characterization was performed using light microscopy equipped with a camera (Leica DMLB, Leica Microsystems GmbH, Wetzlar, Germany) and dynamic image analysis (DIA) (Sync Analyzer, Microtrac Retsch GmbH, Haan, Germany). Microscopic images of cGM batches were captured in both their dry- and PBS-swollen states. DIA measurements were conducted using demineralized water as a dispersant for PBS-swollen batches. For DIA measurements, approximately 10 ml of cGM dispersion (1.5 mg/ml) was introduced into the FlowSync

Table 1
List of experimental runs and oligomer types that were used for the DoE study: DoE runs were based on the optimal design with three factors, including, AC [mmol], TEA [ml] and oligomer MAD [Da]. AC was calculated from the titration data and shows the total amount of anhydride units introduced in the crosslinking reaction via oSMoMA-x. MAD shows the distribution of anhydride units though oligomeric chains. High MAD values indicate low number anhydride units per oligomer chain.

Exp. name	Run order	Oligomer type	AC [mmol] - coded	TEA [ml] - coded	MAD [Da] - coded	AC [mmol]	TEA [ml]	MAD [Da]
N1	N6	oSMoMA-10c	−1	−1	−1	0.93	0.30	316.3
N2	N18	oSMoMA-10c	1	−1	−1	3.04	0.30	316.3
N3	N11	oSMoMA-10c	−1	1	−1	0.93	1.70	316.3
N4	N25	oSMoMA-10c	1	1	−1	3.04	1.70	316.3
N5	N14	oSMoMA-10c	1	1	−1	3.04	1.70	316.3
N6	N3	oSMoMA-10c	−1	−0.333	−1	0.93	0.77	316.3
N7	N2	oSMoMA-10c	−1	0.333	−1	0.93	1.23	316.3
N8	N24	oSMoMA-10c	1	−0.333	−1	3.04	0.77	316.3
N9	N22	oSMoMA-10c	0.333	−1	−1	2.33	0.30	316.3
N10	N10	oSMoMA-10c	−0.333	1	−1	1.63	1.70	316.3
N11	N5	oSMoMA-5	−1	−1	1	0.93	0.30	515.9
N12	N20	oSMoMA-5	1	−1	1	3.04	0.30	515.9
N13	N21	oSMoMA-5	−1	1	1	0.93	1.70	515.9
N14	N29	oSMoMA-5	1	1	1	3.04	1.70	515.9
N15	N15	oSMoMA-5	1	1	1	3.04	1.70	515.9
N16	N27	oSMoMA-5	−1	−0.333	1	0.93	0.77	515.9
N17	N23	oSMoMA-5	−1	0.333	1	0.93	1.23	515.9
N18	N16	oSMoMA-5	1	−0.333	1	3.04	0.77	515.9
N19	N19	oSMoMA-5	−0.333	−1	1	1.63	0.30	515.9
N20	N7	oSMoMA-5	0.333	−1	1	2.33	0.30	515.9
N21	N12	oSMoMA-5	−0.333	1	1	1.63	1.70	515.9
N22	N9	oSMoMA-7.5	−1	−1	−0.278	0.93	0.30	388.4
N23	N26	oSMoMA-7.5	1	−1	−0.278	3.04	0.30	388.4
N24	N8	oSMoMA-7.5	−1	1	−0.278	0.93	1.70	388.4
N25	N1	oSMoMA-7.5	1	0.333	−0.278	3.04	1.23	388.4
N26	N4	oSMoMA-7.5	0.333	1	−0.278	2.33	1.70	388.4
N27	N17	oSMoMA-7.5	0	0	−0.278	1.98	1.00	388.4
N28	N28	oSMoMA-7.5	0	0	−0.278	1.98	1.00	388.4
N29	N30	oSMoMA-7.5	0	0	−0.278	1.98	1.00	388.4
N30	N13	oSMoMA-7.5	0	0	−0.278	1.98	1.00	388.4

unit, and particle images were recorded. Particle shape characterization was based on two shape parameters: sphericity and length-to-width (L/W) aspect ratio (AR), as defined by ISO 9276–6:2008. The mean sphericity and mean L/W aspect ratio (AR) of each batch were used to numerically assess the shape of cGM in the PBS-swollen state. Moreover, DIA was used to evaluate the optical properties of individual PBS-swollen particles, including particle transparency, according to ISO 9276–6:2008 [35]. For each cGM batch, transparency values were calculated on a per-particle basis by the analysis software, and the batch mean particle transparency (MT) was calculated as the arithmetic mean of all analyzed particles within each batch. MT was used as a response variable in the DoE analysis.

2.4.2. Determination of degree of crosslinking of cGM

Degree of crosslinking (DoC) was indirectly quantified using TNBS assay as previously described in the literature [23] with certain modifications. TNBS reacts with free primary amines in the cGM which was subsequently quantified spectrophotometrically. For the assay, the mixture of cGM containing 1 ml of 4 % sodium bicarbonate solution, 4 ml of demineralized water and 1 ml of 0.5 % TNBS solution were incubated in water bath at 40 °C for 4 h. Afterwards, 18 ml of 6 M HCl solution was introduced into the mixture to stop the complexation reaction and hydrolyze the cGM. The reaction mixture was then incubated at 60 °C for additional 1.5 h to ensure cGM hydrolysis and achieve a clear solution. For each batch, the assay included three cGM samples ($n = 3$) and one blank, which contained all reaction components and underwent the same procedure, except that HCl was added at the beginning to prevent complex formation. In the end, absorbance was read at the wavelength of 365 nm. The final absorbance values of cGM were achieved by subtracting absorbance of the blank from the raw absorbance of cGM. The calibration curve using pristine GM was created by the same assay procedure (Fig. S1, supplementary data) and used to calculate DoC as given in Eq. (2).

$$DoC\ [\%] = \left(1 - \frac{ABS_{cGM}}{ABS_{refGM}}\right) \cdot 100 \tag{2}$$

where ABS_{cGM} is the absorbance of cGM and ABS_{refGM} is the absorbance of pristine GM with the same weight (calculated from the calibration curve).

2.5. Design of experiments (DoE)

The DoE consists of three factors: (1) Anhydride content per crosslinking reaction (AC) [mmol]; (2) TEA volume per reaction (TEA) [ml]; (3) Molecular anhydride distribution per oligomer (MAD) [Da]. Oligomer anhydride content per weight (oAC) for each synthesized oligomer batch was calculated using conductometric titration, as previously described [31], and expressed in Eq. (3). Later, for each crosslinking reaction, AC was assured by introducing required weight of oligomer resulting in the predefined AC [mmol] per crosslinking reaction.

$$oAC\left[\frac{mol}{g}\right] = \frac{Oligomer\ anhydride\ mol\ [mol]}{Oligomer\ weight\ [g]} \tag{3}$$

Molecular anhydride distribution (MAD) is an oligomer-specific factor included as structural variable in the DoE. MAD represents a stoichiometric descriptor of anhydride distribution along the oligomer backbone, defined as the number-averaged oligomer chain length per anhydride unit. To determine MAD for each oligomer batch, the molecular anhydride content per oligomer (MAC), defined as the dimensionless number of anhydride units per oligomer backbone, was first calculated from the oligomer anhydride content per weight (oAC) and the oligomer mol per unit mass [mol·g^{-1}] according to Eq. (4).

$$MAC = \frac{\frac{Oligomer\ anhydride\ content\ [mol]}{Oligomer\ weight\ [g]}}{\frac{Oligomer\ mol\ [mol]}{Oligomer\ weight\ [g]}} = \frac{Oligomer\ anhydride\ content\ [mol]}{Oligomer\ mol\ [mol]} \tag{4}$$

Subsequently, MAD was calculated using Eq. (5) as the ratio of the

Table 2
List of oligomer batches and their number averaged molecular weight (M_n), molecular weight dispersity (Đ), their anhydride content per weight (oAC). Batches including, O1, O3 and O5 were used to fabricate preliminary cGM batches while O2, O4 and O6 were used to fabricate cGM batches of DoE runs.

Batch code	Oligomer type	M_n [Da]	Đ	Anhydride content per oligomer weight (oAC) [mmol/g]	Application
O1	oSMoMA-5	2411 ± 22	1.91 ± 0.01	1.86 ± 0.04	Preliminary
O2	oSMoMA-5	2294 ± 39	1.68 ± 0.02	1.94 ± 0.11	DoE
O3	oSMoMA-7.5	1955 ± 08	1.74 ± 0.01	2.34 ± 0.04	Preliminary
O4	oSMoMA-7.5	1783 ± 34	1.67 ± 0.03	2.57 ± 0.16	DoE
O5	oSMoMA-10	1641 ± 04	1.61 ± 0.04	3.04 ± 0.02	Preliminary
O6	oSMoMA-10c	1623 ± 06	1.58 ± 0.01	3.16 ± 0.05	DoE

oligomer M_n to MAC. A higher MAD values correspond to lower stoichiometric density of anhydride units along the oligomer chain, whereas lower MAD values indicate a higher anhydride density.

$$MAD\ [Da]\ = \frac{Oligomer\ M_n\ [Da]}{Molecular\ anhydride\ content\ per\ oligomer} \tag{5}$$

AC and TEA had flexible factor levels that could be easily adjusted. In contrast, MAD was a unique factor, specific to the oligomer batches used in this DoE (Table 1) and was therefore a non-flexible factor with three levels and no center point. Since classical experimental designs could not accommodate such level settings, the optimal design algorithm provided by MODDE 13 Pro software (Version 13.0, Sartorius AG, Göttingen, Germany) was used to generate optimal response-surface design candidates. To minimize confounding between design terms, primarily caused by the asymmetric factor levels of the factor MAD, we specifically selected a design with a high number of experimental runs ($n = 30$). Initially, D-optimization was set as the objective, and multiple full quadratic design candidates were sorted in descending order based on their log(det(X'X)) values. The first two candidates exhibited the highest log(det(X'X)) values of 11.19, with corresponding G-efficiencies of 71.26 %. However, the third design candidate, which had a slightly lower log (det(X'X)) value of 11.16, was selected due to a substantial improvement in G-efficiency, which was 75.91 %. The selected design included three sets of replicates and five levels for the factors AC and TEA. Prior to regression modeling, quantitative factors were centered and orthogonally scaled, resulting in coded experimental variables used for coefficient estimation (Table 1). The correlation matrix of the selected optimal design was provided in the supplementary data (Fig. S2). The responses included batch mean DoC, DoS and MT. Experiments were performed in randomized order and data were fitted using multiple linear regression (MLR) method. Significant effects were determined using analysis of variance (ANOVA) test at 95 % confidence level. Data analysis was carried out using MODDE 13 Pro, whereas data visualization was primarily performed in OriginPro (Version 2024b, OriginLab Corporation, Massachusetts, USA).

3. Results and discussion

3.1. Oligomer characterization

Table 2 presents the number-averaged molecular weights (M_n), molecular weight dispersities (Đ) and anhydride contents per weight [mmol/g] for the oligomer batches used in this study. Some oligomer batches were used for the fabrication of preliminary cGM batches, while the remaining batches were utilized in the fabrication of cGM batches of the DoE runs. Oligomer batches with higher MA feed per synthesis yielded oligomers with smaller M_n. The negative trend between MA feed and M_n indicates that higher molar MA content during radical polymerization led to the formation of oligomers with shorter chains. This was phenomena that was already reported for several former generation anhydride-containing oligomers that were introduced by our group and attributed to the reduced number of charge-transfer complexes (CTCs) in the case of higher MA and lower AMO feed. MA is a reactive electrophilic monomer with minimal tendency toward homopolymerization. In contrast, AMO, acting as an electron donor and good proton acceptor, facilitates the formation of charge-transfer complexes (CTCs) with MA during propagation phase. These CTCs promote efficient alternating copolymerization. Increasing MA content by decreasing AMO is thus expected to lead to less CTC formation, which then would terminate radical polymerization earlier, ultimately leading to oligomers with lower molecular weight [24,31,32,36]. As intended, oligomers synthesized with higher MA feed exhibited higher anhydride content per weight [mmol/g].

Fig. 3 illustrates the ^{1}H NMR spectra of representative oligomer batches for each oligomer type and their peak assignments whereas Table 3 presents the integration details.

Prior to analysis, the I_2 integral area in each ^{1}H—NMR spectrum was normalized to 30 protons, which sets the fatty acid chain of SA as internal standard. Based on this normalization, a set of equations was established to determine the relative molar contents of MA (b_{MA}) and AMO (b_{AMO}) relative to SA (b_{SA} is set to 1). Besides the coefficients b_{MA} and b_{AMO} that determine the molar ratio of MA and AMO to SA in the resulting polymer, we also introduced the scaling factor f that converts the relative NMR-derived comonomer ratios (b-values) into the absolute mass contributions of each comonomer to the individuals co-oligomer molecular weight (Eq. (6)). The factor f consequently also denotes the molar ratio of SA per co-oligomer.

$$M_n\ \left[\frac{g}{mol}\right] = f\cdot(1\cdot M_{SA} + \ b_{AMO}\cdot M_{AMO} + b_{MA}\cdot M_{MA}) \tag{6}$$

The anhydride content per oligomer (oAC) that was determined by titration (Eq. (3)), was converted to the molecular weight contribution of MA groups (M_{CMA}) within an average oligomer molecule (Eq. (7)).

$$M_{CMA}\ \left[\frac{g}{mol}\right] = \left(oAC\ \left[\frac{mol}{g}\right]\cdot M_{MA}\ \left[\frac{g}{mol}\right]\right)\cdot M_n\ (Oligomer)\ \left[\frac{g}{mol}\right] \tag{7}$$

To determine the comonomer composition of the crosslinker oligomers by ^{1}HNMR, we derived Eqs. (8) and (9) using Eq. (6) in combination with M_{CMA}. Eqs. (10) and (11) were derived from peak assignment in the ^{1}H—NMR spectra.

$$f\cdot(1\cdot M_{SA} + \ b_{AMO}\cdot M_{AMO})\ \left[\frac{g}{mol}\right] = M_n - M_{CMA}\ \left[\frac{g}{mol}\right] \tag{8}$$

$$f\cdot(b_{MA}\cdot M_{MA})\ \left[\frac{g}{mol}\right] = M_{CMA}\ \left[\frac{g}{mol}\right] \tag{9}$$

$$9\cdot b_{AMO} + 2\cdot b_{MA} = I_4 - 2 \tag{10}$$

$$11\cdot b_{AMO} + 2\cdot b_{MA} = I_3 + I_4 - 7 \tag{11}$$

These equations were used to calculate f, b_{MA} and b_{AMO}. Table 4 summarizes the results obtained from two calculation approaches: (1) using only integral I_4 to derive the desired information by resolving Eqs. (8), (9) and (10), and (2) employing both I_3 and I_4 to determine the proton numbers according to Eqs. (8), (9) and (11). Both approaches were evaluated, as each is subject to experimental bias. Approach 1 requires subtraction of the water signal despite incomplete baseline separation during the integration of I_4. Approach 2 additionally includes

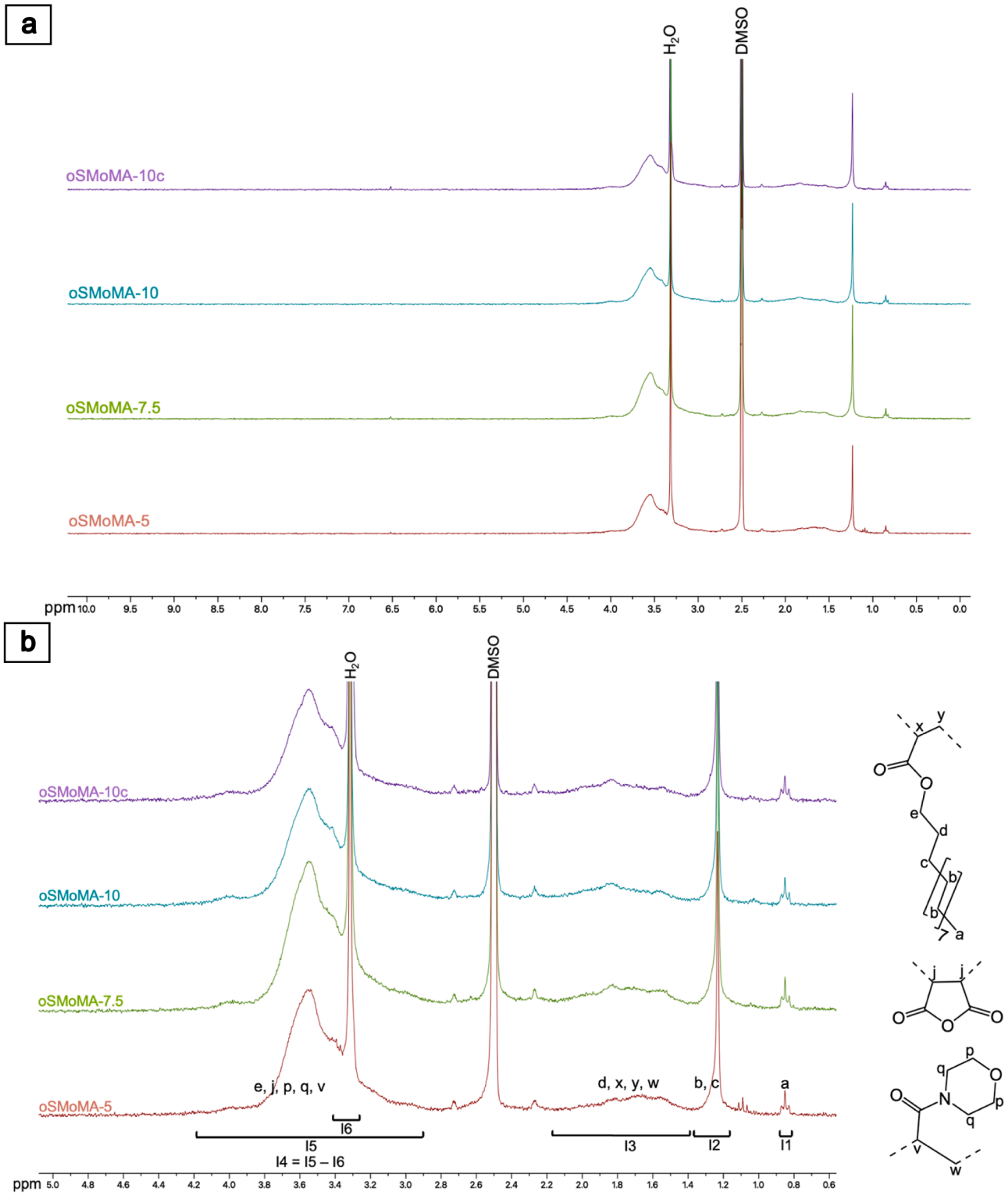

Fig. 3. Peak assignments of ^{1}H NMR spectra of representative oligomer batches for each oligomer type: (a) Overall spectra, (b) Zoomed spectra and peak assignments. From bottom to top, each spectrum belongs to batch code of O1, O3, O5 and O6, respectively (Table 2 for oligomer batch codes). The protons were labeled with letters, and each letter was assigned to the corresponding peak. ^{1}H NMR measurements were conducted at 300 MHz frequency (Bruker Avance III - 300, Bruker BioSpin GmbH, Ettlingen, Germany) using dimethyl sulfoxide-d6 (DMSO-d6) as a solvent at a sample concentration of 2.5 mg/ml. Prior to evaluation, each raw ^{1}H NMR spectrum was processed using MNova software (version: 14.2.0, Mestrelab Research, S.L.U., Barcelona, Spain). Spectrum processing was performed using following steps: (1) Line smoothing (Whittaker method), (2) Manual phase correction and (3) Auto-baseline correction. Prediction tool in the software was used for peak assignments.

Table 3
Integration details and number of theoretical protons for each comonomer per integral area.

Integral name	Integration range [ppm]	Number of theoretical protons assigned for each integral area		
		SA	MA	AMO
I_1	0.81 – 0.89	3	0	0
I_2	1.15 – 1.35	30	0	0
I_3	1.38 – 2.17	5	0	2
I_4	[2.90 – 3.26) ∪ (3.43 – 4.18]	2	2	9

the protons of I_3 to compensate for errors arising from water-signal extraction but tends to overestimate the protons contributing to I_3, since the integrated peaks are located on an elevated baseline (Fig. 3).

In comparison to the theoretical feed ratios (Table 4), both analytical approaches indicated a higher incorporation of MA and AMO relative to SA, which is consistent with previous observations. During radical polymerization, SA is presumed to exhibit lower reactivity than the comonomers MA and, in particular, AMO. The incorporation of MA, represented by b_{MA}, was generally close to the theoretical feed ratios across all oligomer batches for both approaches. The deviation between the theoretical AMO/SA feed ratio (theoretical b_{AMO}) and the calculated b_{AMO} increased for oligomers synthesized with higher MA feed ratios, such as oSMoMA-10. At high AMO feeds, e.g. for a theoretical b_{AMO} of 10, AMO homooligomerization is promoted, yielding calculated values of 14.54 using the first approach and 15.46 using the second approach. As intended, this deviation was less pronounced for oSMoMA-10c, in which AMO was introduced gradually over 2 h, allowing for improved stoichiometric control over the copolymerization.

Similar deviations have been reported previously for anhydride-containing oligomers, where proton signal ratios were influenced by oligomer type and MA content. Loth et al. and Krieghoff et al. analyzed oligo(PEDAS-*co*-NiPAAm-*co*-MA) using $CDCl_3$/DMSO-d_6 (2:1 v/v) as NMR solvent and, consistent with our first approach, derived the NiPAAm/PEDAS ratio from a single integral [31,36]. Their results showed higher experimental than theoretical ratios for oligomers synthesized with elevated MA feed (oPNMA-7.5 and oPNMA-10). This trend was also reported for DAAm/PEDAS systems [32] and is now likewise observed for the AMO/SA (b_{AMO}) ratios in this study.

3.2. GM crosslinking process

3.2.1. Preliminary experiments

Fig. 4 presents the plots, created from preliminary cGM batches. Higher DoC [%] was achieved with oligomers that contained more anhydride groups per weight [mmol/g] and with the use of higher oligomer concentrations (Fig. 4a). Furthermore, a non-linear trend was observed when the same data were expressed as a function of AC used per crosslinking reaction [mmol] and DoC [%] (Fig. 4b). This trend was expected since the crosslinking reaction approaches saturation at high crosslinking densities, likely due to the reduced availability of free amine groups as crosslinking progresses. Subsequently, applying the natural logarithm to AC linearized the data (Fig. 4c), indicating that the observed correlation follows a logarithmic regression.

These initial observations suggested that quadratic effects might be significant in the crosslinking process when DoC is used as the response, providing initial insights for our DoE planning. In addition, the linearization of AC through ln-transformation became of interest in the DoE study. Therefore, for the response DoC, we also evaluated the current design using ln(AC) as a factor, referring to this model as the "ln(AC) model". The model using AC as a factor was referred to as the "AC model".

3.2.2. Design of experiments (DoE)

3.2.2.1. Descriptive overview of DoE study. Fig. 5 illustrates the design

Table 4
Molar ratio of comonomers calculated through ^{1}HNMR integrations, GPC and titration results. In ^{1}HNMR spectra, SA protons were normalized using I_2 area to 30 protons. Molar content of AMO in the end was calculated either from I_4 or from I_3 and I_4.

Oligomer batch	Theoretical reaction feed molar ratios			Comonomer composition – calculated molar ratios					
				calculated from Integral I_4			calculated from integrals I_3 and I_4		
	SA	MA	AMO	AMO/SA (b_{AMO})	MA/SA (b_{MA})	f	AMO/SA (b_{AMO})	MA/SA (b_{MA})	f
oSMoMA-5	1.0	5.0	15.0	16.7	6.1	0.74	17.2	6.3	0.72
oSMoMA-7.5	1.0	7.5	12.5	15.6	7.7	0.60	16.5	8.1	0.57
oSMoMA-10	1.0	10.0	10.0	14.5	10.3	0.49	15.5	10.8	0.46
oSMoMA-10c	1.0	10.0	10.0	12.8	9.8	0.53	13.8	10.4	0.49

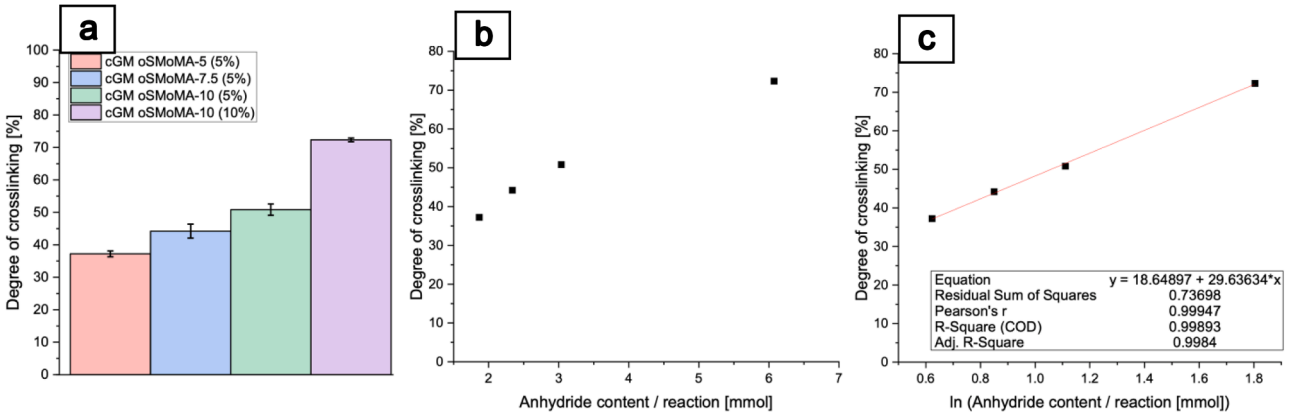

Fig. 4. cGM fabricated in experiments preceding the DoE series. Plots (a) - (c) show the same cGM degree of crosslinking (DoC) data plotted as a function of (a) oligomer type and concentration, (b) anhydride content used per crosslinking reaction (AC), which exhibits a nonlinear AC-DoC relationship, and (c) ln-transformed anhydride content (ln(AC)), resulting in a logarithmic DoC-ln(AC) relationship.

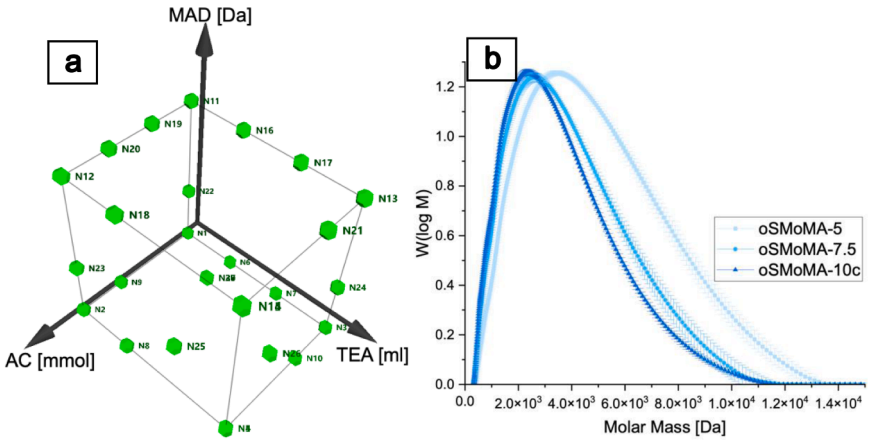

Fig. 5. (a) Illustration of the design region of the experimental runs of the optimal design. The design region was generated from coded factor levels, and corresponding non-coded values as provided in Table 1. (b) Molar mass distribution of oligomer batches that were used to fabricate cGM of the DoE runs.

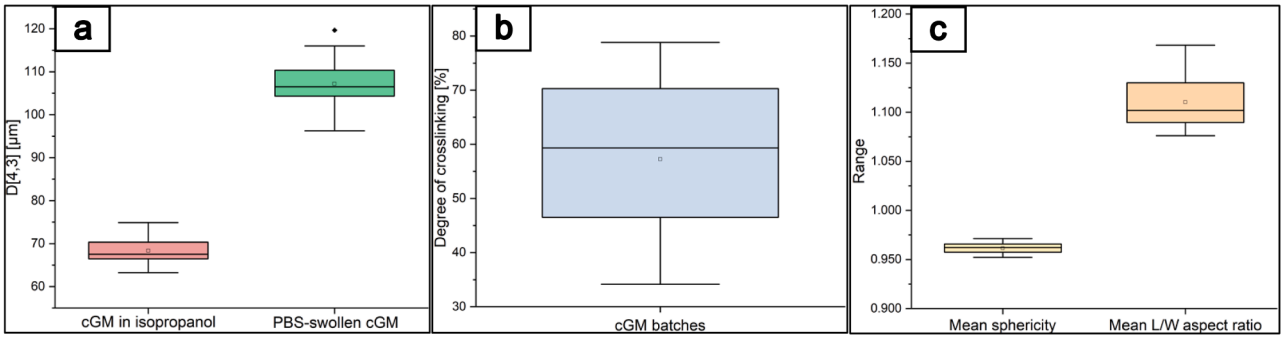

Fig. 6. Overview of particle size, shape, and crosslinking characteristics of cGM batches obtained from the DoE runs. (a) Box-whisker plot of the de Brouckere mean diameter (D[4,3]) of all cGM batches of DoE runs at dry-state (particles dispersed in isopropanol) and at swollen-state (particles swollen in PBS); (b) Box-whisker plot of batch degree of crosslinking of cGM batches of DoE runs ($n = 30$) and (c) Box-whisker plot of batch mean sphericity and mean L/W AR of PBS swollen-cGM batches of DoE runs. Boxes and whiskers indicate the 25–75 and 1–99 percentiles, respectively.

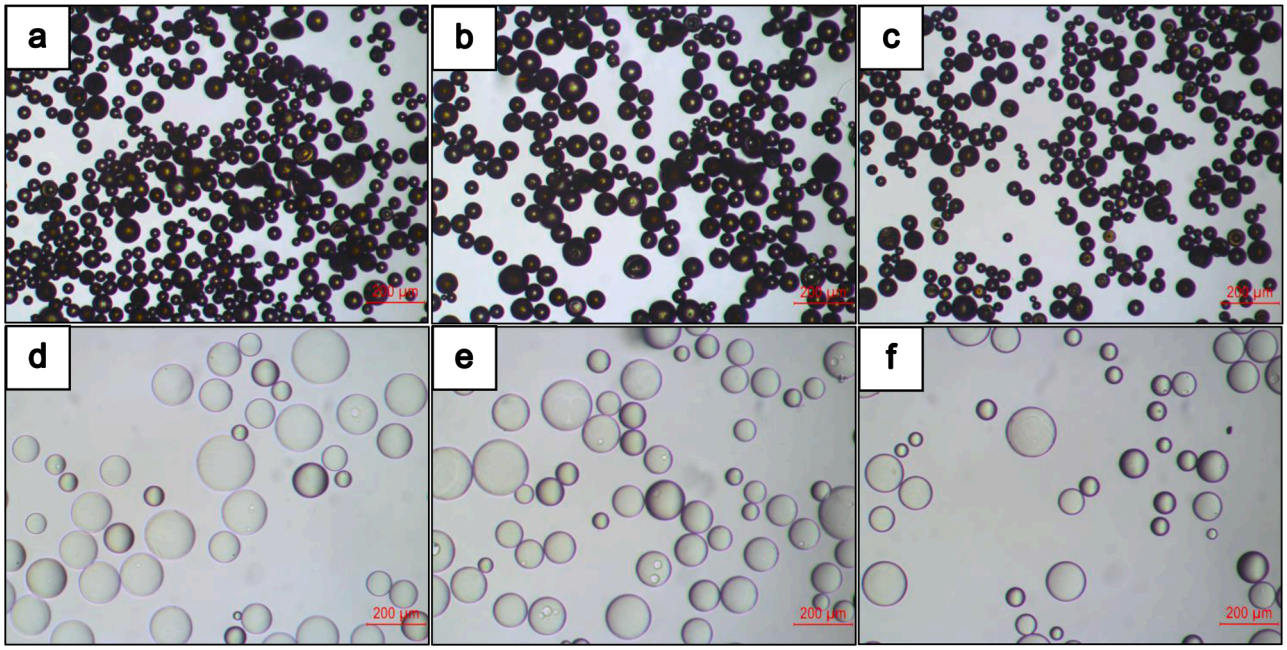

Fig. 7. Light micrographs of cGM batches representing low, medium and high crosslinking density. (a) cGM batch "N16" in dry state, degree of crosslinking: 34.15 ± 1.13 %; (b) cGM batch "N18" in dry state, degree of crosslinking: 59.68 ± 1.22 %; (c) cGM batch "N8" in dry state, degree of crosslinking: 78.82 ± 1.65 %; (d) cGM batch "N16" in PBS-swollen state; (e) cGM batch "N18" in PBS-swollen state and (f) cGM batch "N8" in PBS-swollen state.

Table 5
List of model terms and metrics, obtained for each response before and after model tuning. AC: anhydride content per crosslinking reaction [mmol]; TEA: triethylamine volume used per crosslinking reaction [ml] and MAD: molecular anhydride distribution [Da].

List of model terms								
AC model								
Response	**Before model tuning**				**After model tuning**			
DoC [%]	*AC, TEA, MAD, AC·AC, TEA·TEA, MAD·MAD, AC·TEA, AC·MAD, TEA·MAD*				*AC, TEA, MAD, AC·AC, TEA·TEA, MAD·MAD, AC·TEA*			
DoS	*AC, TEA, MAD, AC·AC, TEA·TEA, MAD·MAD, AC·TEA, AC·MAD, TEA·MAD*				*AC, TEA, MAD, MAD·MAD, TEA·MAD*			
MT	*AC, TEA, MAD, AC·AC, TEA·TEA, MAD·MAD, AC·TEA, AC·MAD, TEA·MAD*				*AC, TEA, MAD, AC·AC, TEA·TEA, MAD·MAD, AC·TEA, TEA·MAD*			
ln(AC) model								
DoC [%]	*ln(AC), TEA, MAD,* ln*(AC)·* ln*(AC), TEA·TEA, MAD·MAD,* ln*(AC)·TEA,* ln*(AC)·MAD, TEA·MAD*				*ln(AC), TEA, MAD, TEA·TEA, MAD·MAD,* ln*(AC)·TEA*			
Model metrics								
AC model								
Response	**R^2**	**Q^2**	**Model validity**	**Model reproducibility**	**R^2**	**Q^2**	**Model validity**	**Model reproducibility**
DoC [%]	0.960	0.902	0.951	0.914	0.959	0.921	0.962	0.914
DoS	0.669	0.266	0.939	0.358	0.639	0.436	0.948	0.358
MT	0.804	0.542	0.950	0.578	0.804	0.592	0.958	0.578
ln(AC) model								
DoC [%]	0.958	0.896	0.940	0.914	0.954	0.919	0.950	0.914

region for the selected "optimal design" and the molecular mass distribution of oligomer batches used to fabricate DoE batches. For oSMoMA-5, synthesized with a low MA feed, the resulting oligomer exhibited relatively longer chain lengths and broader molecular mass distributions, whereas increasing the MA feed during synthesis yielded oligomers with shorter chains and narrower molecular mass distributions.

Fig. 6 illustrates Box-Whisker plots of responses related to particle size, shape, and DoC for the cGM batches of the DoE study. The mean D [4,3] of non-swollen cGM (measured in isopropanol) ranged from 63 to 75 μm, while after swelling in PBS, the mean D[4,3] increased to a range of 98 to 120 μm across the DoE batches (Fig. 6a). The DoC of the DoE batches indicates that, with the current factor-level combinations, we achieved particles with a broad range of crosslinking densities, allowing for a comprehensive analysis of this response (Fig. 6b). The maximum degree of cGM crosslinking achieved in this study with oSMoMA-x was comparable to the highly crosslinked cGM reported for conventional crosslinkers such as glutaraldehyde [37] and genipin [9], as well as earlier-generation anhydride-containing crosslinkers like oPNMA-x [23]. Highly crosslinked GM prepared with anhydride-containing oligomers may exhibit increased surface acidity, which could influence cell-material interactions in tissue-engineering applications [38,39]. However, elevated crosslinking densities can also be advantageous for drug-delivery strategies, for example by enabling macrophage-mediated microparticle degradation associated with drug release [40]. Therefore, the demonstrated capability to precisely tune the DoC over a broad range constitutes a key advantage for rational and application-oriented material design.

In our previous work, we conducted an extensive study on the fabrication of pristine GM, focusing on controlling particle size distribution and shape. Particle shape quality was evaluated based on two morphological parameters: sphericity and length-to-width (L/W) aspect ratio [33]. In the present study, particle shape analysis of PBS-swollen cGM batches revealed predominantly spherical morphologies across the DoE batches, although certain batches exhibited higher L/W aspect ratios, likely due to increased agglomeration tendencies after crosslinking. Nonetheless, all batches showed mean sphericity values exceeding 0.95, confirming that the crosslinking process did not alter particle morphology. Spherical particle shape was further supported by light micrographs presented in Fig. 7, showing exemplary batches across varying crosslinking densities. Notably, most particles appeared even more spherical, particularly after PBS swelling. These results highlight the importance of controlling particle shape quality during the initial GM fabrication process [33], and suggest that unlike conventional crosslinkers such as GTA [23], post-fabrication crosslinking step using oSMoMA-x as a crosslinker has no negative impact on particle shape.

3.2.2.2. DoE model development and statistical evaluation. Table 5 summarizes the model terms for both full quadratic and tuned models, along with the metrics obtained after tuning. The response DoC exhibited a good model fit and high predictive power for both the AC and ln(AC) models, before and after model tuning. In contrast, the models for DoS and MT showed weaker fits, reflected by lower prediction power (Q^2) values and reproducibility. These deviations were mainly driven by batches N14 and N29, which likely experienced experimental inconsistencies but were nevertheless retained in the datasets.

Additional residual analyses, provided in the supplementary data (Fig. S3) confirmed generally random residual distributions with minor deviations from normality. The lower Q^2 values observed for DoS and MT are attributed to the nature of these responses as indirect indicators of network structure, which exhibited lower reproducibility across replicate runs compared to the chemically sensitive TNBS-based DoC determination. Although DoC values are obtained from bulk particle samples, the TNBS assay provides a direct quantitative assessment of crosslinking. In contrast, DoS and MT represent physical responses derived from particle size and optical measurements obtained via laser diffraction and dynamic image analysis. While these analytical methods themselves are highly reproducible, the calculated responses are more sensitive to distribution effects and agglomeration tendencies, whereas the DoS response additionally reflects variability propagation associated with its ratio-based calculation. Notably, model tuning improved prediction power, particularly for DoS. Variability related to analytically derived factors such as AC and MAD may also contribute to residual variation. Since both parameters were calculated from experimentally-determined oligomer properties (oAC and M_n), analytical variability is unavoidable. However, comparable variability across oligomer batches (Table 2) indicates that the relative separation between factor levels remained robust across different oligomer types within experimental limits, suggesting that potential variations in MAD did not compromise the overall DoE interpretation. Overall, the model validity was high across all investigated responses.

3.2.2.3. Analysis and interpretation of DoE effects

DoE effects on crosslinking behavior of GM. In order to understand the crosslinking behavior of GM, the effects of individual DoE factors were first interpreted through the DoC response. Coefficient plots for the models developed through the DoE were shown in Fig. 8. For the response DoC, Fig. 8a compares the coefficients of the AC model and the ln(AC) model. The quadratic effect of AC, which was significant in the AC model, became insignificant in the ln(AC) model. This finding further supports our preliminary data (Fig. 4) that the AC-DoC relationship follows a logarithmic regression, suggesting progressive saturation of accessible gelatin amines relative to the available anhydride content

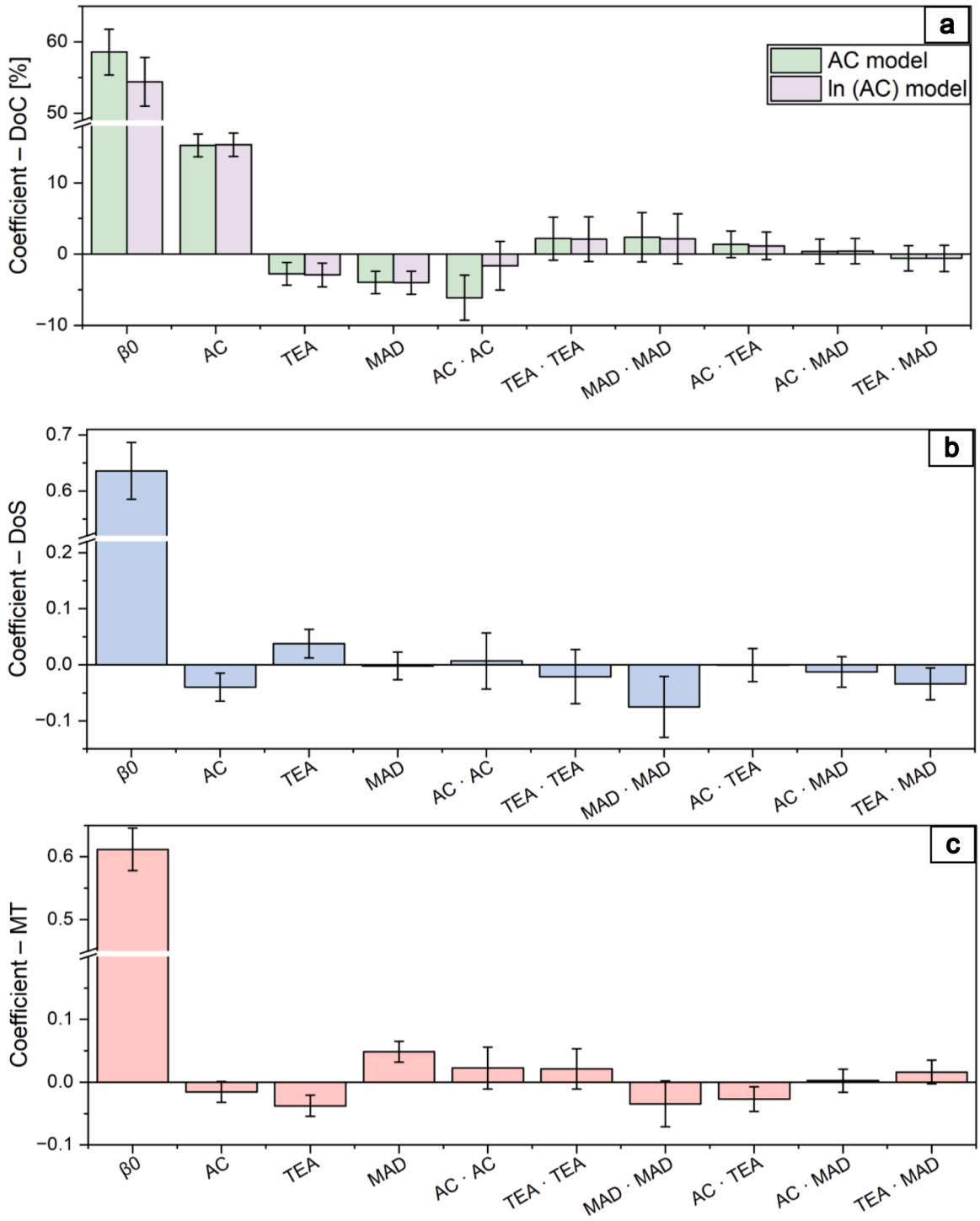

Fig. 8. Scaled and centered coefficient plots of non-tuned full quadratic models derived for each response. Coefficients for AC-based and ln(AC)-based models are shown for direct comparison; AC terms shown on the x-axis correspond to ln(AC) terms in the ln(AC) model. (a) Batch mean degree of crosslinking (DoC) [%]; (b) batch mean degree of swelling (DoS); (c) batch mean particle transparency (MT). AC: anhydride content per crosslinking reaction [mmol]; TEA: triethylamine volume [ml]; MAD: molecular anhydride distribution [Da]. Coefficients are shown as means with 95 % confidence intervals.

during the crosslinking process. In addition, the coefficients of the other design terms were comparable between the AC and ln(AC) models, indicating that a logarithmic transformation of AC had minimal influence on the remaining model terms. Comparable saturation effects between crosslinker amount and crosslinking density have been reported in GA-crosslinked bulk gelatin hydrogel systems, where limited accessibility of reactive sites and diffusion constraints may restrict further increases in crosslinking at higher crosslinker levels [41]. However, quantitative descriptions of saturation-type crosslinking behavior remain scarce in the GM literature. The data obtained in the present study substantiate a logarithmic relationship between AC and DoC, thereby providing an improved quantitative description of this saturation behavior for GM crosslinked with the investigated anhydride-containing oligomer system within the explored design region. On the other hand, negative main effect of AC on the responses DoS and MT indicate that at high AC conditions, particles swell less and

become less transparent likely, due to their higher particle crosslinking density. For the response DoS, AC showed almost no quadratic effect. Therefore, under the current factor level combinations, particle swelling seems to follow a linear trend with AC, the factor with highest effect on particle crosslinking density.

In contrast to AC, the significant negative main effect of TEA volume on DoC suggests that the crosslinking reaction may be hindered at higher pH values. As the positive quadratic effect of TEA on DoC appeared insignificant, it can be assumed that the reaction is negatively affected under conditions exceeding a certain pH threshold. Since our crosslinking method involves water to facilitate GM swelling, we assume that highly basic environments resulting from elevated TEA content may accelerate the hydrolysis kinetics of anhydride units. Typically, the amide formation in the crosslinking reaction is expected to proceed faster than anhydride hydrolysis at neutral pH. However, due to the diffusion barrier of the GM matrix through which oligomeric crosslinkers must diffuse in a time-dependent manner, hydrolysis kinetics may influence the resulting DoC. The effect of pH on hydrolysis kinetics of cyclic anhydride-containing oligomers or copolymers has not been extensively investigated in the literature. However, early kinetic studies indicate that anhydride hydrolysis in aqueous media is accelerated under basic conditions (pH $>$ 8) for certain small molecules, such as phthalic anhydride [42] and naphthalic anhydride [43].

Mechanistic interpretation and material implications of DoE results. To further interpret the DoE results in terms of network structure and material behavior, the effects of individual factors on particle swelling (DoS) and optical properties (MT) were examined. Contrary to its effect on DoC, TEA volume showed a significant positive main effect for DoS, indicating that particles crosslinked with higher TEA volume exhibited greater swelling. This outcome was expected, as lower crosslinking density renders the crosslinked gelatin network more flexible at the molecular level, leading to enhanced particle swelling. Such behavior aligns with classical hydrogel swelling concepts, where lower crosslinking density reduces the elastic constraints of the polymer network [44], enabling greater swelling of the matrix upon equilibrium water uptake. The negative effect of crosslinking density on cGM swelling has likewise been reported in several other studies involving different types of crosslinkers, including glutaraldehyde, genipin [37], D,L-glyceraldehyde [26] and 3-glycidoxypropyltrimethoxysilane [3]. From a quality-by-design (QbD) perspective, controlling crosslinking density and swelling behavior is critical, as these parameters govern degradation characteristics and thereby influence CQAs such as drug-release profiles in gelatin-based microparticle systems [3,45–47]. Finally, the negative main effect of TEA on MT may indicate that the crosslinking pattern varies with TEA levels. As a proton scavenger, TEA influences the degree of deprotonation of amines in gelatin chains. At higher TEA levels, a greater fraction of primary amine group may become reactive toward anhydrides, potentially altering the local distribution of crosslinks within the particle matrix, which could influence light scattering and thereby reduce particle transparency. This behavior is also consistent with the coefficients of the response DoS, suggesting that optical properties are sensitive to local network topology rather than solely to the average swelling behavior of the particles.

Factor MAD represents the distribution of anhydride units along oligomeric chains. Higher MAD values correspond to fewer anhydride units per Dalton of oligomer chain length, indicating lower stoichiometric density of anhydride units within oligomer chains. During gelatin crosslinking with anhydride-containing oligomers, the number of anhydride units participating in the crosslinking reaction is a critical parameter for final material design. Each unreacted anhydride group will eventually hydrolyze, generating two carboxylic acid groups per unit, whereas anhydride-amine coupling yields a single carboxyl group adjacent to an amide linkage [14,23]. The outcomes of anhydride units participating in crosslinking versus undergoing hydrolysis, and their implications for the microenvironmental pH of the final cGM, were schematically illustrated in Fig. S4 (supplementary data). The formation of additional carboxylic acid groups due to unreacted anhydride units is anticipated to lower the microenvironmental pH of the final cGM, potentially imposing limitations on the material design. For instance, acidic microenvironments have been reported to inhibit osteoblast proliferation [38] and to decrease cell viability while affecting cell morphology in macrophages [39]. Since the stoichiometric anhydride density per oligomer chain length might affect the number of anhydrides reacting with gelatin amines, MAD was considered as a critical material attribute for the crosslinking process. The significant negative main effect of MAD on DoC indicated that the crosslinking density was reduced for oligomers with lower anhydride density along the oligomer chains. This effect can also be related to diffusion challenges upon crosslinking as there is a correlation between MAD and oligomer molecular weight. Oligomer batches with higher MAD also exhibited larger chain lengths (higher M_n), which likely diffuse into GM more slowly than those with lower MAD and lower molecular weight. Oligomers with high MAD (and concomitant high M_n) may less freely reach deeper layers of the particles limiting the access of anhydride units to gelatin amines. As previously established, longer diffusion times may also correlate with increased anhydride hydrolysis and ultimately result in reduced crosslinking densities of the matrix network.

The significant negative quadratic effect of MAD on the response DoS reveals that particle swelling was greater within a certain MAD range, whereas cGM crosslinked with oligomers at either high or low MAD exhibited restricted swelling. This outcome was expected for cGM crosslinked with oligomers with low MAD, as a higher number of anhydride units distributed per unit oligomer chain length likely promoted more frequent amine-anhydride conjugation, ultimately restricting the swelling capacity of the final cGM. Interestingly, swelling was also slightly restricted at high MAD levels. Consistent with the diffusion-related considerations discussed above, slower transport of longer oligomer chains at high MAD may promote heterogeneous crosslinking during particle penetration. Such heterogeneous network formation may introduce locally denser regions that limit chain mobility and impose localized elastic constraints within the gelatin matrix, thereby constraining macroscopic swelling even in cGM with relatively lower DoC. These results suggest that MAD not only influences the overall swelling behavior but also modulates the network structure of the cGM matrix, which is also reflected in the optical properties of the swollen particles. Positive significant main effect of MAD on MT suggests that particles become more transparent once crosslinking is achieved through longer oligomer chains with lower anhydride density. However, the negative quadratic effect of MAD also reveals that MT is particularly reduced when oligomers with lower MAD values are used. In addition, the positive interaction effect (TEA·MAD), which was close to significance, suggests that increased amine reactivity at high TEA levels enhances MAD-dependent differences in network structure, making MT particularly sensitive to variations in MAD under these conditions. Details of the factor-response relationships are further visualized through response contour plots presented in Fig. S5 (supplementary data).

These results highlight the importance of considering MAD as a factor in future crosslinking processes, particularly for material designs that involve oligomer pre-derivatization prior to crosslinking. For instance, Hinkelmann et al. derivatized 25 mol % of intact anhydride units in the oligomer oPNMA-7.5 using *N,N*-diethylethylenediamine prior to its use in crosslinking. This modification was designed to introduce positively charged functional groups into the final cGM, thereby enhancing its cell-attachment properties when applied as a microtissue assembly platform [13,14]. However, partial consumption of anhydride units prior to crosslinking alters MAD, which may in turn affect the crosslinking process. Therefore, MAD can be considered as an additional factor in such processes in the future to achieve cGM with the desired DoC. In addition, unlike the same studies where cGM were fabricated with relatively high TEA volumes [13,14], our results demonstrated that cGM with a broad range of DoC can be effectively produced using minimal TEA volumes, a favorable outcome since

Table 6
Summary of DoE factors, response trends and mechanistic interpretation of process behavior and material properties.

Category	Parameter	Response trends	Mechanistic interpretation	Key material and process conclusion
DoE factor	Anhydride content (AC)	Strong positive main effect on DoC; higher AC associated with reduced particle swelling (DoS) and transparency (MT)	Increasing AC increases the availability of reactive anhydride groups, promoting amine-anhydride coupling until progressive saturation of accessible gelatin amines occurs	AC is the primary driver controlling crosslinking density; logarithmic AC-DoC behavior indicates saturation-controlled network formation, implying that relatively high DoC can be achieved already at moderate AC levels within the explored design region, which is favorable for efficient use of such crosslinkers
DoE factor	TEA volume (TEA)	Negative main effect on DoC; positive main effect on DoS and MT	Elevated TEA increases pH and may promote anhydride hydrolysis, affecting DoC, while altered gelatin amine deprotonation can modify local crosslinking patterns within cGM particle volume, reflected in MT.	Low TEA levels are sufficient to achieve broad DoC ranges; minimizing TEA is advantageous to reduce hydrolysis and potential cytotoxicity risks due to residual TEA
DoE factor	Molecular anhydride distribution (MAD)	Negative main effect on DoC; quadratic influence on DoS; positive main effect on MT	Higher MAD reflects longer oligomer chains with lower stoichiometric anhydride density, reducing effective diffusivity and multi-point crosslink formation during reaction-diffusion-coupled network development within GM.	MAD serves as an oligomer-specific structural descriptor linking oligomer structure to diffusion behavior, amine-anhydride encounter probability, and the balance between crosslinking and anhydride hydrolysis; particularly for cGM intended for tissue-engineering applications, it should be considered as a design factor when targeting defined DoC levels, as oligomer pre-derivatization prior to GM crosslinking alters MAD.
Response-response interpretation	DoC-property relationship	Higher DoC associated with reduced DoS and MT	Increased network density imposes elastic constraints on the gelatin matrix and enhances light scattering within swollen particles	Crosslinking density defines network structure, with swelling and transparency acting as indicators, supporting targeted control of degradation and drug-release behavior in drug delivery and tissue-engineering applications.

residual TEA may exert hazardous effects on cells. Finally, in this study we introduced AC as a factor rather than using oligomer weight or percentage, which have previously been used as key process parameters. This approach provides greater flexibility in controlling the DoC of the final cGM, particularly when new oligomers with varying anhydride content are used in the future. Table 6 summarizes the relationships between investigated factors, observed response trends, and their mechanistic implications for the resulting material properties.

4. Conclusion

The present work systematically investigated the crosslinking process of GM with a new generation oligomeric anhydride-containing crosslinkers, oSMoMA-x, using DoE statistics. Batches of cGM were effectively fabricated with a broad range of DoC, comparable to those obtained with conventional crosslinkers and earlier-generation anhydride-containing crosslinkers. The spherical shape of GM was maintained during crosslinking which was confirmed by dynamic image analysis and light micrographs, demonstrating that the crosslinking strategy did not considerably alter particle morphology. Moreover, in this study, oligomer AC was introduced for the first time as a factor, rather than controlling the process through oligomer weight or concentration. AC was found to have an effect with highest magnitude on particle DoC, and AC logarithmically correlated with DoC. A general trend between DoC and DoS was also noticeable, suggesting that particle swelling was reduced by denser crosslinking. The TEA volume used in the crosslinking reactions showed that low levels are sufficient to achieve a broad range of DoC. Therefore, future studies should consider employing lower TEA. The anhydride distribution along the oligomers indirectly reflects the stoichiometric density of anhydride units along the oligomer chains. Through DoE, MAD was established as a critical material attribute for this process, as it exhibited significant effects on all responses. Therefore, we recommend that MAD be considered as a factor in future studies, not only for prospective new-generation oligomers but also for strategies that involve oligomer pre-derivatization. To our knowledge, this is the first study to investigate cGM crosslinking by amine-anhydride conversion using DoE statistics, providing process insights to guide future studies employing prospective crosslinkers in cGM fabrication.

CRediT authorship contribution statement

Burak Demir: Conceptualization, Formal analysis, Investigation, Methodology, Visualization, Writing – original draft, Writing – review & editing. **Johannes Reiss:** Methodology. **Julia C. Matros:** Methodology. **Stefan Klinken-Uth:** Methodology. **Michael C. Hacker:** Conceptualization, Formal analysis, Funding acquisition, Methodology, Supervision, Writing – review & editing.

Declaration of competing interest

The authors declare that they have no known competing financial interests or personal relationships that could have appeared to influence the work reported in this paper.

Acknowledgments

The authors thank Jan Krieghoff (Leipzig University, Institute of Pharmacy) for reliable oligomer characterization by GPC.

Supplementary materials

Supplementary material associated with this article can be found, in the online version, at doi:10.1016/j.rineng.2026.109860.

Data availability

Data will be made available on request.

References

[1] B. Behrend-Keim, A. Castro-Munoz, L. Monrreal-Ortega, B. Avalos-Leon, C. Campos-Estrada, H.D.C. Smyth, T.F. Bahamondez-Canas, D. Moraga-Espinoza, The forgotten material: highly dispersible and swellable gelatin-based microspheres for pulmonary drug delivery of cromolyn sodium and ipratropium

bromide, Int. J. Pharm. 644 (2023) 123331, https://doi.org/10.1016/j.ijpharm.2023.123331.
[2] S. Cao, L. Li, Y. Du, J. Gan, J. Wang, T. Wang, Y. Liu, W. Liu, Y. Zhou, X. Gao, H. Li, T. Liu, Porous gelatin microspheres for controlled drug delivery with high hemostatic efficacy, Colloids Surf. B Biointerfaces 207 (2021) 112013, https://doi.org/10.1016/j.colsurfb.2021.112013.
[3] M. Nouri-Felekori, M. Khakbiz, N. Nezafati, J. Mohammadi, M.B. Eslaminejad, Comparative analysis and properties evaluation of gelatin microspheres crosslinked with glutaraldehyde and 3-glycidoxypropyltrimethoxysilane as drug delivery systems for the antibiotic vancomycin, Int. J. Pharm. 557 (2019) 208–220, https://doi.org/10.1016/j.ijpharm.2018.12.054.
[4] T.H. Tran, T. Ramasamy, B.K. Poudel, N. Marasini, B.K. Moon, H.J. Cho, H.-G. Choi, C.S. Yong, J.O. Kim, Preparation and characterization of spray-dried gelatin microspheres encapsulating ganciclovir, Macromol. Res. 22 (2) (2013) 124–130, https://doi.org/10.1007/s13233-014-2018-9.
[5] T.T. Lau, C. Wang, D.-A. Wang, Cell delivery with genipin crosslinked gelatin microspheres in hydrogel/microcarrier composite, Compos. Sci. Technol. 70 (13) (2010) 1909–1914, https://doi.org/10.1016/j.compscitech.2010.05.015.
[6] N. Contessi Negrini, M.V. Lipreri, M.C. Tanzi, S. Fare, In vitro cell delivery by gelatin microspheres prepared in water-in-oil emulsion, J. Mater. Sci. Mater. Med. 31 (3) (2020) 26, https://doi.org/10.1007/s10856-020-6363-2.
[7] M. Shi, Y. Gao, L. Lee, T. Song, J. Zhou, L. Yan, Y. Li, Adaptive gelatin microspheres enhanced stem cell delivery and integration with diabetic wounds to activate skin tissue regeneration, Front. Bioeng. Biotechnol. 10 (2022) 813805, https://doi.org/10.3389/fbioe.2022.813805.
[8] Z.S. Patel, M. Yamamoto, H. Ueda, Y. Tabata, A.G. Mikos, Biodegradable gelatin microparticles as delivery systems for the controlled release of bone morphogenetic protein-2, Acta Biomater. 4 (5) (2008) 1126–1138, https://doi.org/10.1016/j.actbio.2008.04.002.
[9] P.A. Turner, J.S. Thiele, J.P. Stegemann, Growth factor sequestration and enzyme-mediated release from genipin-crosslinked gelatin microspheres, J. Biomater. Sci. Polym. Ed. 28 (16) (2017) 1826–1846, https://doi.org/10.1080/09205063.2017.1354672.
[10] J. Yang, M. Zhou, W. Li, F. Lin, G. Shan, Preparation and evaluation of sustained release platelet-rich plasma-loaded gelatin microspheres using an emulsion method, ACS Omega 5 (42) (2020) 27113–27118, https://doi.org/10.1021/acsomega.0c02543.
[11] H. Nakase, K. Okazaki, Y. Tabata, M. Ozeki, N. Watanabe, M. Ohana, S. Uose, K. Uchida, T. Nishi, M. Mastuura, H. Tamaki, T. Itoh, C. Kawanami, T. Chiba, New cytokine delivery system using gelatin microspheres containing interleukin-10 for experimental inflammatory bowel disease, J. Pharmacol. Exp. Ther. 301 (1) (2002) 59–65, https://doi.org/10.1124/jpet.301.1.59.
[12] A.K. Kudva, A.D. Dikina, F.P. Luyten, E. Alsberg, J. Patterson, Gelatin microspheres releasing transforming growth factor drive in vitro chondrogenesis of human periosteum derived cells in micromass culture, Acta Biomater. 90 (2019) 287–299, https://doi.org/10.1016/j.actbio.2019.03.039.
[13] S. Hinkelmann, A.H. Springwald, S. Schulze, U. Hempel, F. Mitrach, C. Wolk, M. C. Hacker, M. Schulz-Siegmund, Mineralizing gelatin microparticles as cell carrier and drug delivery system for siRNA for bone tissue engineering, Pharmaceutics 14 (3) (2022), https://doi.org/10.3390/pharmaceutics14030548.
[14] S. Hinkelmann, A.H. Springwald, A. Starke, H. Kalwa, C. Wolk, M.C. Hacker, M. Schulz-Siegmund, Microtissues from mesenchymal stem cells and siRNA-loaded cross-linked gelatin microparticles for bone regeneration, Mater. Today Bio 13 (2022) 100190, https://doi.org/10.1016/j.mtbio.2021.100190.
[15] R. Cortesi, E. Esposito, E. Menegatto, R. Gambari, C. Nastruzzi, Gelatin microspheres as a new approach for the controlled delivery of synthetic oligonucleotides and PCR-generated DNA fragments, Int. J. Pharm. 105 (2) (1994) 181–186, https://doi.org/10.1016/0378-5173(94)90464-2.
[16] Y. Obata, T. Nishino, T. Kushibiki, R. Tomoshige, Z. Xia, M. Miyazaki, K. Abe, T. Koji, Y. Tabata, S. Kohno, HSP47 siRNA conjugated with cationized gelatin microspheres suppresses peritoneal fibrosis in mice, Acta Biomater. 8 (7) (2012) 2688–2696, https://doi.org/10.1016/j.actbio.2012.03.050.
[17] Q. Li, Y. Deng, X. Liu, Delivering multifunctional peptide-conjugated gene carrier/miRNA-218 complexes from monodisperse microspheres for bone regeneration, ACS Appl. Mater. Interfaces 14 (38) (2022) 42904–42914, https://doi.org/10.1021/acsami.2c10728.
[18] Y. Qian, Y. Gu, F. Tribukait-Riemenschneider, I. Martin, V.P. Shastri, Incorporation of cross-linked gelatin microparticles to enhance cell attachment and chondrogenesis in carboxylated agarose bioinks for cartilage engineering, ACS Appl. Mater. Interfaces 17 (15) (2025) 22293–22307, https://doi.org/10.1021/acsami.5c00077.
[19] L.D. Solorio, E.L. Vieregge, C.D. Dhami, P.N. Dang, E. Alsberg, Engineered cartilage via self-assembled hMSC sheets with incorporated biodegradable gelatin microspheres releasing transforming growth factor-beta1, J. Control Release 158 (2) (2012) 224–232, https://doi.org/10.1016/j.jconrel.2011.11.003.
[20] C. Fan, S.H. Zhan, Z.X. Dong, W. Yang, W.S. Deng, X. Liu, D.A. Wang, P. Sun, Cross-linked gelatin microsphere-based scaffolds as a delivery vehicle of MC3T3-E1 cells: in vitro and in vivo evaluation, Mater. Sci. Eng. C Mater. Biol. Appl. 108 (2020) 110399, https://doi.org/10.1016/j.msec.2019.110399.
[21] M. Foox, M. Zilberman, Drug delivery from gelatin-based systems, Expert. Opin. Drug Deliv. 12 (9) (2015) 1547–1563, https://doi.org/10.1517/17425247.2015.1037272.
[22] C.E. Campiglio, N. Contessi Negrini, S. Fare, L. Draghi, Cross-linking strategies for electrospun gelatin scaffolds, Materials 12 (15) (2019), https://doi.org/10.3390/ma12152476. . (Basel).
[23] T. Loth, R. Hotzel, C. Kascholke, U. Anderegg, M. Schulz-Siegmund, M.C. Hacker, Gelatin-based biomaterial engineering with anhydride-containing oligomeric cross-linkers, Biomacromolecules 15 (6) (2014) 2104–2118, https://doi.org/10.1021/bm500241y.
[24] H.A. Nawaz, K. Schrock, M. Schmid, J. Krieghoff, I. Maqsood, C. Kascholke, C. Kohn-Polster, M. Schulz-Siegmund, M.C. Hacker, Injectable oligomer-cross-linked gelatine hydrogels via anhydride-amine-conjugation, J. Mater. Chem. B 9 (9) (2021) 2295–2307, https://doi.org/10.1039/d0tb02861d.
[25] N. Adhirajan, N. Shanmugasundaram, M. Babu, Gelatin microspheres cross-linked with EDC as a drug delivery system for doxycyline: development and characterization, J. Microencapsul. 24 (7) (2008) 659–671, https://doi.org/10.1080/02652040701500137.
[26] M.A. Vandelli, F. Rivasi, P. Guerra, F. Forni, R. Arletti, Gelatin microspheres crosslinked with d,l-glyceraldehyde as a potential drug delivery system: preparation, characterisation, in vitro and in vivo studies, Int. J. Pharm. 215 (1) (2001) 175–184, https://doi.org/10.1016/S0378-5173(00)00681-5.
[27] S. Sulaiman, R.A. Rani, N.H. Mohamad Yahaya, Y. Tabata, Y. Hiraoka, W.T. Seet, M.H. Ng, Physical and natural crosslinking approaches on three-dimensional gelatin microspheres for cartilage regeneration, Tissue Eng. Part C Methods 28 (10) (2022) 557–569, https://doi.org/10.1089/ten.tec.2022.0073.
[28] G. Yang, Z. Xiao, H. Long, K. Ma, J. Zhang, X. Ren, J. Zhang, Assessment of the characteristics and biocompatibility of gelatin sponge scaffolds prepared by various crosslinking methods, Sci. Rep. 8 (1) (2018) 1616, https://doi.org/10.1038/s41598-018-20006-y.
[29] Z. Wang, H. Liu, W. Luo, T. Cai, Z. Li, Y. Liu, W. Gao, Q. Wan, X. Wang, J. Wang, Y. Wang, X. Yang, Regeneration of skeletal system with genipin crosslinked biomaterials, J. Tissue Eng. 11 (2020) 2041731420974861, https://doi.org/10.1177/2041731420974861.
[30] C. Kohn-Polster, B.M. Müller, J. Krieghoff, A. Nawaz, I. Maqsood, A. Starke, K. Haastert-Talini, M. Schulz-Siegmund, M.C. Hacker, Functionalization of two-component gelatinous peptide/reactive oligomer hydrogels with small molecular amines for enhanced cellular interaction, Int. J. Mol. Sci. 26 (11) (2025) 5316, https://doi.org/10.3390/ijms26115316.
[31] T. Loth, R. Hennig, C. Kascholke, R. Hötzel, M.C. Hacker, Reactive and stimuli-responsive maleic anhydride containing macromers – multi-functional cross-linkers and building blocks for hydrogel fabrication, React. Funct. Polym. 73 (11) (2013) 1480–1492, https://doi.org/10.1016/j.reactfunctpolym.2013.08.002.
[32] C. Kascholke, T. Loth, C. Kohn-Polster, S. Moller, P. Bellstedt, M. Schulz-Siegmund, M. Schnabelrauch, M.C. Hacker, Dual-functional hydrazide-reactive and anhydride-containing oligomeric hydrogel building blocks, Biomacromolecules 18 (3) (2017) 683–694, https://doi.org/10.1021/acs.biomac.6b01355.
[33] B. Demir, M.C. Hacker, Critical process parameters of gelatin microparticle fabrication with a water-in-oil emulsion method, Int. J. Pharm. 686 (2025) 126302, https://doi.org/10.1016/j.ijpharm.2025.126302.
[34] S.H.P. Bettini, J.A.M. Agnelli, Evaluation of methods used for analysing maleic anhydride grafted onto polypropylene by reactive processing, Polym. Test. 19 (1) (2000) 3–15, https://doi.org/10.1016/S0142-9418(98)00066-X.
[35] IOf Standardization, ISO 9276-6: Representation of Results of Particle Size Analysis — Part 6: Descriptive and Quantitative Representation of Particle Shape and Morphology, ISO, Geneva, Switzerland, 2008.
[36] J. Krieghoff, J. Rost, C. Kohn-Polster, B.M. Muller, A. Koenig, T. Flath, M. Schulz-Siegmund, F.P. Schulze, M.C. Hacker, Extrusion-printing of multi-channeled two-component hydrogel constructs from gelatinous peptides and anhydride-containing oligomers, Biomedicines 9 (4) (2021), https://doi.org/10.3390/biomedicines9040370.
[37] H.C. Liang, W.H. Chang, K.J. Lin, H.W. Sung, Genipin-crosslinked gelatin microspheres as a drug carrier for intramuscular administration: in vitro and in vivo studies, J. Biomed. Mater. Res. A 65 (2) (2003) 271–282, https://doi.org/10.1002/jbm.a.10476.
[38] C. Ruan, N. Hu, Y. Ma, Y. Li, J. Liu, X. Zhang, H. Pan, The interfacial pH of acidic degradable polymeric biomaterials and its effects on osteoblast behavior, Sci. Rep. 7 (1) (2017) 6794, https://doi.org/10.1038/s41598-017-06354-1.
[39] H. Wu, Y. Yin, X. Hu, C. Peng, Y. Liu, Q. Li, W. Huang, Q. Huang, Effects of environmental pH on macrophage polarization and osteoimmunomodulation, ACS Biomater. Sci. Eng. 5 (10) (2019) 5548–5557, https://doi.org/10.1021/acsbiomaterials.9b01181.
[40] R.T. Annamalai, P.A. Turner, W.F. Carson, B. Levi, S. Kunkel, J.P. Stegemann, Harnessing macrophage-mediated degradation of gelatin microspheres for spatiotemporal control of BMP2 release, Biomaterials 161 (2018) 216–227, https://doi.org/10.1016/j.biomaterials.2018.01.040.
[41] K. Iwanaga, T. Yabuta, M. Kakemi, K. Morimoto, Y. Tabata, Y. Ikada, Usefulness of microspheres composed of gelatin with various cross-linking density, J. Microencapsul. 20 (6) (2003) 767–776, https://doi.org/10.3109/02652040309178087.
[42] G.O. Andrés, A.M. Granados, R.H. de Rossi, Kinetic study of the hydrolysis of phthalic anhydride and aryl hydrogen phthalates, J. Org. Chem. 66 (23) (2001) 7653–7657, https://doi.org/10.1021/jo010499v.
[43] T.C. Barros, S. Yunes, G. Menegon, F. Nome, H. Chaimovich, M.J. Politi, L.G. Dias, I.M. Cuccovia, Hydrolysis of 1,8- and 2,3-naphthalic anhydrides and the mechanism of cyclization of 1,8-naphthalic acid in aqueous solutions, J. Chem. Soc. Perkin Trans. 2 (12) (2001) 2342–2350, https://doi.org/10.1039/b104148g.
[44] N.R. Richbourg, N.A. Peppas, The swollen polymer network hypothesis: quantitative models of hydrogel swelling, stiffness, and solute transport, Prog. Polym. Sci. 105 (2020) 101243, https://doi.org/10.1016/j.progpolymsci.2020.101243.

[45] Y.B. Choy, F. Cheng, H. Choi, K. Kim, Monodisperse gelatin microspheres as a drug delivery vehicle: release profile and effect of crosslinking density, Macromol. Biosci. 8 (8) (2008) 758–765, https://doi.org/10.1002/mabi.200700316.
[46] A.H. Nguyen, J. McKinney, T. Miller, T. Bongiorno, T.C. McDevitt, Gelatin methacrylate microspheres for controlled growth factor release, Acta Biomater. 13 (2015) 101–110, https://doi.org/10.1016/j.actbio.2014.11.028.
[47] J. Wang, Y. Tauchi, Y. Deguchi, K. Morimoto, Y. Tabata, Y. Ikada, Positively charged gelatin microspheres as gastric mucoadhesive drug delivery system for eradication of H. pylori, Drug Deliv. 7 (4) (2000) 237–243, https://doi.org/10.1080/107175400455173.